PHYSICAL REVIEW C **93**, 041303(R) (2016)

Luneburg-lens-like universal structural Pauli attraction in nucleus-nucleus interactions: Origin of emergence of cluster structures and nuclear rainbows

S. Ohkubo
Research Center for Nuclear Physics, Osaka University, Ibaraki, Osaka 567-0047, Japan
(Received 29 February 2016; published 21 April 2016)

The Pauli exclusion principle plays an important role in many-body fermion systems, preventing them from collapsing by repulsion. For example, the Pauli principle causes a repulsive potential at short distances between two α particles. On the other hand, the existence of nuclear rainbows demonstrates that the internuclear potential is sufficiently attractive in the internal region to cause refraction. The two concepts of repulsion and attraction are seemingly irreconcilable. Contrary to traditional understanding, it is shown that the Pauli principle causes a *universal structural Pauli attraction* between nuclei rather than a *structural repulsive core*. Through systematic studies of $\alpha+\alpha$, $\alpha+{}^{16}$O, $\alpha+{}^{40}$Ca, and ^{16}O$+{}^{16}$O systems, it is shown that the emergence of cluster structures near the threshold energy at low energies and nuclear rainbows at high energies is a direct consequence of the Pauli principle.

DOI: 10.1103/PhysRevC.93.041303

Why do cluster structures appear near the threshold energy, while molecular resonances occur at higher excitation energies, and nuclear rainbows at even high energies? The threshold rule, molecular resonance theory, and nuclear rainbow theory have been proposed and extensively studied for more than fifty years. Until now, these independent theories—each describing successfully different facets of nuclear structure—had not been thought to be closely connected at the level of a fundamental principle. I will show that they share a common *raison d'être*: They are all a direct consequence of the universal Pauli attraction.

The Pauli exclusion principle plays an important role in nuclei. The shell structure, in which nucleons behave like independent particles in a mean field potential and persist throughout the periodic table, is a consequence of the Pauli principle and the short-range character of the nuclear force [1]. The Pauli principle also plays an important role between nuclei at small distances where they overlap. For the typical $\alpha+\alpha$ system, microscopic resonationg group method (RGM) studies have revealed [2–5] that the internuclear interaction for S and D waves has a *repulsive* core at short distances and angular-momentum (L) dependent *shallow* attraction in the outer region. The repulsive core explains the experimental phase shifts in $\alpha+\alpha$ scattering and the well-developed α cluster structure of ^{8}Be well [3–6]. The repulsive core was found to be a potential representation of the damped inner oscillations of the intercluster wave functions, with the energy-independent node at around 2 fm caused by the Pauli principle [4,5]. This is known as the *structural repulsive core* [7]. For heavy-ion systems such as ^{16}O$+{}^{16}$O, the existence of a repulsive core at short distances has also been shown in microscopic model calculations [8–10].

Although the so-called standard optical potential model with a Woods-Saxon form factor witnessed tremendous success in the studies of light-ion and heavy-ion scattering and reactions [11], it could not describe the backward angle anomaly (BAA) or anomalous large angle scattering (ALAS) in $\alpha+{}^{16}$O and $\alpha+{}^{40}$Ca scattering [12]. This was shown to be resolved using a *nonstandard* optical model with a *deep* potential without a repulsive core, for $\alpha+{}^{16}$O in Refs. [13,14] and for $\alpha+{}^{40}$Ca in Refs. [15,16]. Furthermore the clear observation of the Airy minimum of the nuclear rainbow in ^{16}O$+{}^{16}$O scattering at $E_L=350$ MeV [17] showed that the potential is *deep* in the internal region [18]. The deep potentials in the internal region from the ALAS and rainbow are inconsistent with the repulsive core picture concluded from the microscopic studies.

On the other hand, the deep potentials are found to be similar to a double folding model potential derived from an effective two-body force. One might thus naively understand that the deep potentials, hence the ALAS and nuclear rainbow phenomena, may be a consequence of the strong attractive nature of the nuclear forces. However, in contrast to traditional understanding, I will show that the deep potentials, and therefore also the emergence of a nuclear rainbow and nuclear clustering, are a direct consequence of the Pauli principle.

The purpose of this paper is to show that the Pauli principle between nuclei causes a strong Luneburg-lens-like *universal structural Pauli attraction* in the internal region, which is in contrast to the traditional understanding that the Pauli principle causes a repulsive core at short distances. The Luneburg-lens-like universal Pauli attraction allows the emergence of the simultaneous existence of cluster structures near the threshold energy in the low excitation energy region and a nuclear rainbow in the high energy region.

In composite particle scattering, absorption is mostly strong, which makes it difficult to determine the potential up to the internal region without ambiguity. However, there are some exceptions where absorption is weak or incomplete, and the nuclear rainbow and ALAS, in which scattering waves penetrate deep into the internal region, are observed in elastic scattering. $\alpha+{}^{16}$O [13,14,19] and $\alpha+{}^{40}$Ca [15,16,19–21] scattering are such typical examples, for which a global potential, which works over a wide range of energies, has been determined.

In Fig. 1 the angular distribution in $\alpha+{}^{40}$Ca scattering at $E_L=61$ MeV, calculated using a global potential with a Woods-Saxon squared form factor (thick solid line), which

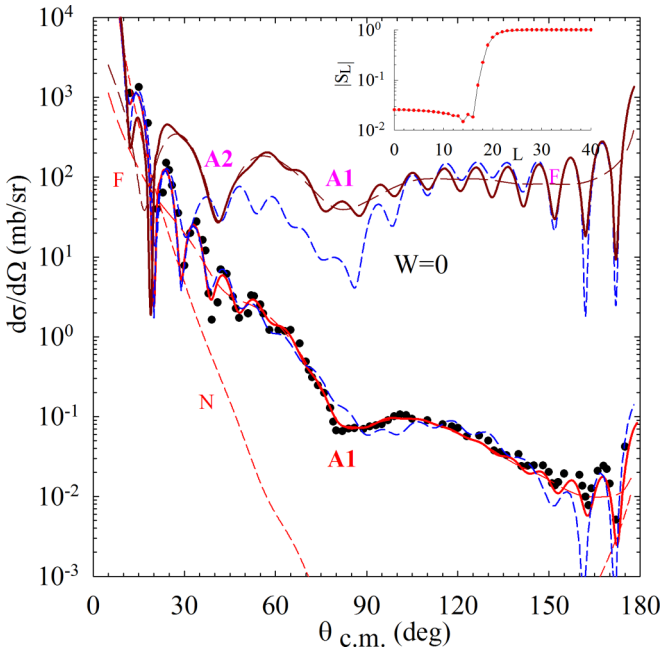

FIG. 1. The experimental angular distribution (points) [16] in $\alpha + {}^{40}$Ca rainbow scattering at $E_L = 61$ MeV and the calculated one (red thick solid line), which is decomposed into the farside (red long-dashed line) and nearside (red medium-dashed line) contributions. The moduli of S matrices, $|S_L|$, in the inset (red filled circles) are connected by lines to guide the eye. The angular distribution (brown thin solid line) and its farside component (brown long-dashed line) calculated by switching off the imaginary potential ($W = 0$) are also displayed. The cutoff calculations of $L = 0$–11 partial waves with and without W are shown by the blue short-dashed lines.

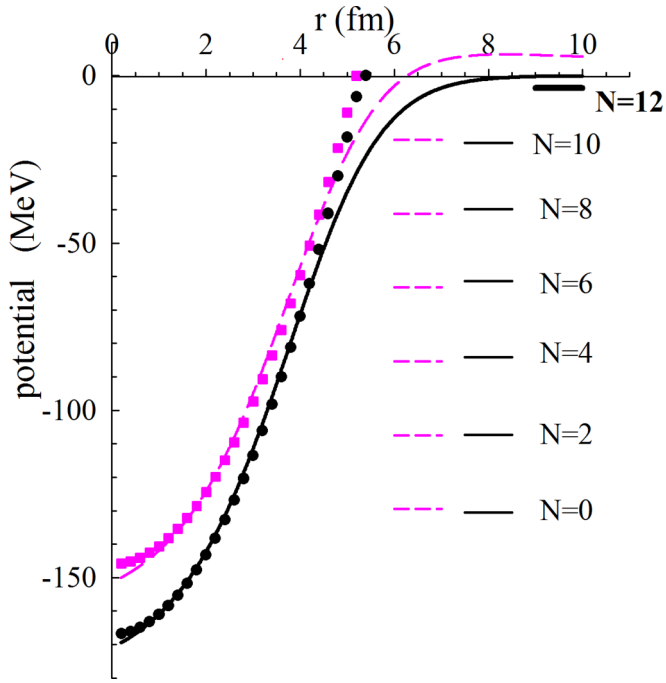

FIG. 2. The global nuclear potential (black solid lines) and the corresponding Luneburg lens potential (black circles) for the $\alpha + {}^{40}$Ca system. The potential including the Coulomb potentials and corresponding Luneburg lens potential are indicated by long-dashed lines (pink) and squares (pink), respectively. The calculated eigenstates for $L = 0$ with $N < N_0 = 12$ together with the $N = N_0$ band head 0^+ of the $\alpha + {}^{40}$Ca cluster state in ^{44}Ti are indicated by horizontal solid lines. The eigenenergies of the Luneburg potential including the Coulomb potential are indicated by horizontal dashed lines.

works well over a wide range of energies $E_L = 24$–166 MeV [16], is compared with the experimental data. The decomposition of the calculated cross sections into the farside and nearside components shows that the minimum at around $\theta = 80^\circ$ is caused by farside refractive scattering and is the first-order Airy minimum $A1$ of the nuclear rainbow. The global potential can be uniquely determined by reproducing the Airy structure of the nuclear rainbow. The calculations in which the imaginary potential is switched off ($W = 0$) show that the minimum at around $\theta = 40^\circ$ is a remnant of the Airy minimum $A2$, and the broad bump in the experimental angular distribution in the $\theta = 40^\circ$–80° region is a remnant of the $A2$ Airy maximum. The moduli of the S matrices, $|S_L|$, which for $L = 0$–11 is of the order of 10^{-2} (inset), shows that absorption is relatively weak. This makes the observation of a nuclear rainbow possible. The cutoff calculations for the smaller L values, $L = 0$–11 (short dashed line), show that these partial waves contribute to the correct description of the Airy structure, which is also confirmed in the same calculations with $W = 0$ (short dashed line). The global potential also reproduces well the ALAS [16], the $\alpha + {}^{40}$Ca fusion oscillations in the lower energy region $E_L = 10$–27 MeV [22], and the α cluster structure in ^{44}Ti including the energy levels, $B(E2)$ values, and α spectroscopic factors [19,20,23,24]. The semimicroscopic double folding potentials derived from the effective two-body Hasegawa-Nagata-Yamamoto (HNY) force [25] and the density-dependent M3Y (DDM3Y) force [26] are similar to the global potential and describe the $\alpha + {}^{40}$Ca system over a wide range of energies as well [21,27].

In Fig. 2 the global potential (solid lines) used in Ref. [20], D180 with the potential strength -180 MeV, and the potential including the Coulomb potential (long dashed lines) are displayed. The internal region of these potentials resembles the truncated harmonic oscillator (HO) potential well, which is called a Luneburg lens potential, as displayed by the filled circles (black) and squares (pink), respectively. The depth $-V_0$ and the truncation radius R, at which the HO potential is zero, are $V_0 = 167$ MeV and $R = 5.3$ fm for the nuclear potential only and $V_0 = 146$ MeV and $R = 5.2$ fm for the combined nuclear and Coulomb potential. In Fig. 2 the states with $N < N_0 = 12$ are Pauli forbidden, where $N \equiv 2n + L$, with n being the number of the nodes in the wave functions. The $N = 12$ state corresponds to the ground state with the $\alpha + {}^{40}$Ca cluster structure in ^{44}Ti. The eigenenergies of the truncated HO potential (horizontal dashed lines) correspond well to those of the global potential. In Table I the overlap of the calculated wave functions with $N < N_0$ in the global potentials with the redundant Pauli forbidden HO wave functions is almost complete. This means that the redundant Pauli forbidden states of the RGM equations are almost completely embedded in the

TABLE I. The overlap of the calculated wave functions of the $L = 0$ bound states for $N < N_0$ with the redundant Pauli forbidden HO wave functions with the oscillator parameters $\nu = 0.535$, 0.32, 0.284, and 0.292 fm^{-2} for $\alpha + \alpha$, $\alpha + {}^{16}$O, $\alpha + {}^{40}$Ca, and ^{16}O$+{}^{16}$O, respectively. $\nu = m\omega/\hbar$, with m being the nucleon mass. $-V_0$ is the strength of the combined nuclear and Coulomb potentials near the origin, $r = 0.01$ fm, in Figs. 2, 3(b), 4, and 5.

System	N_0	V_0 (MeV)	$N=0$	$N=2$	$N=4$	$N=6$	$N=8$	$N=10$	$N=12$	$N=14$	$N=16$	$N=18$	$N=20$	$N=22$
$\alpha+\alpha$	4	119	0.99	0.99										
$\alpha+{}^{16}$O	8	134	0.99	0.98	0.99	0.98								
$\alpha+{}^{40}$Ca	12	151	1.00	1.00	1.00	1.00	0.99	0.93						
^{16}O$+{}^{16}$O	24	321	0.98	0.93	0.91	0.89	0.89	0.91	0.93	0.96	0.96	0.90	0.74	0.43

global potential. The situation is almost the same for the other $L < N_0 - 2n$.

This is true for other systems. In Fig. 3(a) the experimental angular distribution in $\alpha + {}^{16}$O rainbow scattering at $E_L = 49.5$ MeV is compared with the one calculated using the phenomenological global potential, which was determined from the systematic analysis of the ALAS and nuclear rainbow scattering [14]. The Airy structure with the Airy minimum $A1$ at around $\theta = 75^\circ$ followed by the broad Airy maximum $A1$ is well reproduced by the global potential. The Airy structure is brought about by the farside refractive scattering. Furthermore, using the technique in Refs. [28,29], the Airy structure is found to be caused by the interference between the two subamplitudes, i.e., the farside-subcomponent of the internal waves, which penetrate the potential barrier at the surface into the internal region, and the farside-subcomponent of the barrier waves, which are reflected at the barrier. In fact, in the inset of Fig. 3(a) the moduli of the S matrix of the internal waves calculated using the technique in Ref. [28] are significantly large. If one cuts off the contributions of the partial waves for $L = 0$–7 (blue medium-dashed lines), the Airy minimum is destroyed in disagreement with the experiment. This means the waves with smaller L values contribute to the correct reproduction of the Airy structure, i.e., to constraining the shape and depth of the potential in the internal region. In Fig. 3(b) the global potential for the $\alpha + {}^{16}$O system with the energy-dependent parameter $\alpha = 3.02$ in Ref. [14] is shown. This potential, which reproduces well the observed α cluster structure in ^{20}Ne, the energy levels, $B(E2)$ values, and α widths [14,19], resembles the semimicroscopic double folding potentials derived from the HNY force (triangles in Fig. 3) [13,14] and the DDM3Y force [30,31] well. The internal region of the global potential (solid line) is well simulated by the Luneburg lens truncated HO potential with $V_0 = 131$ MeV and $R = 3.75$ fm (filled circles) and, when the Coulomb potential is added (long dashed line), with $V_0 = 144$ MeV and $R = 3.9$ fm (filled squares). The $N = 8$ state corresponds to the ground state with the $\alpha + {}^{16}$O cluster structure in ^{20}Ne. Table I shows that the overlap of the wave functions of the states with $N < 8$ and the redundant Pauli forbidden HO wave functions is almost complete.

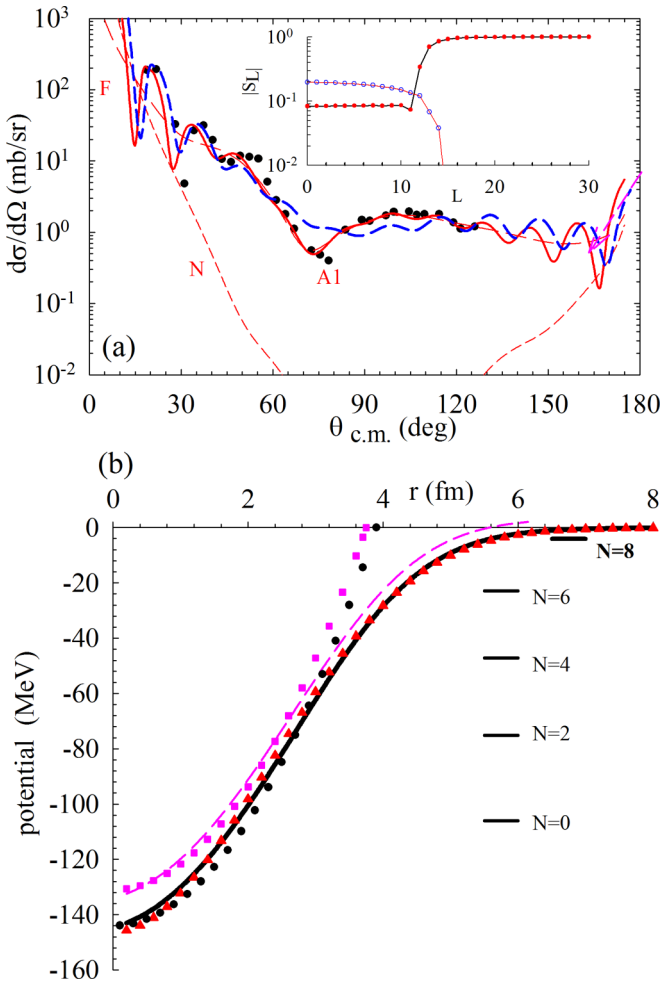

FIG. 3. Same as Fig. 1 for panel (a) and Fig. 2 for panel (b) but for the $\alpha + {}^{16}$O system with $N_0 = 8$. In the inset of panel (a) $|S_L|$ of the internal waves are additionally indicated by unfilled circles. In panel (b) the triangles (red) are the double folding potentials derived from the HNY force with -538 MeV for the triplet even state in the intermediate range [25]. The $N = 8$ (solid horizontal line) shows the $\alpha + {}^{16}$O cluster ground state in ^{20}Ne.

In Fig. 4 the global potential for $\alpha + \alpha$ [10], which reproduces the experimental phase shifts of elastic scattering over a wide range of energies, is displayed. The internal region of the potential without (with) the Coulomb potential is well simulated by the truncated HO potential with $V_0 = 120$ MeV and $R = 2.5$ fm (116 MeV and 2.4 fm). In Fig. 5 the global potential for ^{16}O$+{}^{16}$O in Ref. [32] is displayed. The global potential reproduces the rainbow scattering [17,18,29,33,34] and molecular structure with the ^{16}O$+{}^{16}$O cluster structure in a unified way [32]. The internal region of the potentials resembles the Luneburg lens truncated HO potentials well,

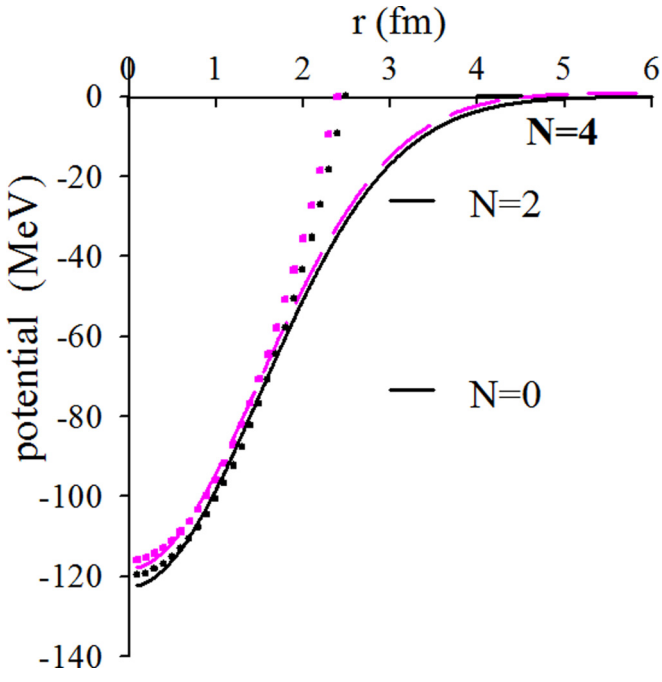

FIG. 4. Same as Fig. 2 but for the $\alpha+\alpha$ system with $N_0=4$. The solid horizontal line shows the $N=4$ ground state with $\alpha+\alpha$ cluster structure in ^{8}Be.

with $V_0=266$ MeV and $R=4.7$ fm when the Coulomb potential is included and with 310 MeV and 4.8 fm for the nuclear potential only. For the ^{16}O+^{16}O system it is noted that the region $r<2$ fm has some ambiguity and the slightly different folding potential in this region can reproduce the ^{16}O+^{16}O scattering equally well [34]. In Table I the overlap of the states for $N<N_0$ with the redundant Pauli forbidden HO

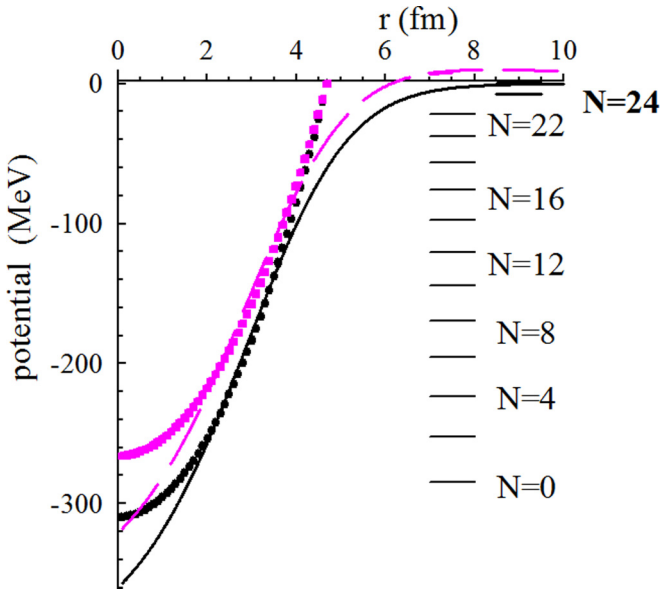

FIG. 5. Same as Fig. 2 but for the ^{16}O+^{16}O system with $N_0=24$. The solid horizontal line shows the $N=24$ 0^+ state with ^{16}O+^{16}O cluster structure in ^{32}S.

wave functions is large except for $N=22$ near the threshold energy.

Thus the physical wave functions with $N\geqslant N_0$ generated by the global potentials are found to be orthogonal to the redundant Pauli forbidden HO wave functions in the RGM. This orthogonality is closely related to the shape and depth of the potential in the internal region, i.e., the Luneburg-lens-like truncated HO potential. I will now show theoretically that the global potentials have a Luneburg-lens-like universal Pauli attraction in the internal region. The RGM equation for the antisymmetrized wave function for two clusters that are assumed to have HO shell model wave functions with size parameter ν and spin 0 is given by

$$[T_r+V_D(r)-E]\chi_L(r)+\int K(r,r')dr'\chi_L(r')=0, \qquad (1)$$

where $\chi_L(r)$, T_r, $V_D(r)$, E, and $K(r,r')$ are the relative wave function, kinetic energy operator of the relative motion, direct (double folding) potential, relative energy, and exchange kernel, respectively. Since one knows that the local potential works very well, if one approximates $K(r,r')=V_P(r)\delta(r-r')$, Eq. (1) becomes a local potential equation

$$\{T_r+V_D(r)+V_P(r)-E\}\chi_L(r)=0, \qquad (2)$$

with the local potential $V(r)\equiv V_D(r)+V_P(r)$. One can impose the eigenfunctions $\chi_L^{(n)}(r)$ with $n<(N_0-L)/2$ to satisfy

$$\{T_r+V_{\rm HO}(r)-(2n+L+3/2)\hbar\omega\}\chi_L^{(n)}(r)=0, \qquad (3)$$

where $V_{\rm HO}(r)$ is the HO potential with a depth $-V_0$ at $r=0$ and the size parameter ν. This guarantees that the physical wave functions of Eq. (2) with $N\geqslant N_0$ are orthogonal to the redundant Pauli forbidden states. This is satisfied when $V(r)=V_{\rm HO}(r)$ in the internal region $r<R$, where R is the size of the Luneburg lens, which is a HO potential truncated at $r=R$ as given below. Thus in order that the wave functions of the physical states satisfy the Pauli principle, the local potential should resemble a deep HO potential in the internal region, i.e., a Luneburg lens potential. When the $V_D(r)$ itself resembles a deep HO as seen for the HNY force (triangles) in Fig. 3(b), the $V_P(r)$ is small [13]. On the other hand, when $V_D(r)$ is repulsive (in the case of, for example, Brink-Boeker force B1), the $V_P(r)$ must be deep so that the $V(r)$ resembles a Luneburg lens potential. Thus the Pauli principle plays the role generating a $V_P(r)$ so that the $V(r)$ resembles a Luneburg lens like HO potential in the internal region.

A Luneburg lens with a radius R is a lens that refracts all the parallel incident trajectories to the focus R_f ($<R$). For such a lens the refractive index n is given by

$$n^2(r\leqslant R)=\left(R_f^2-r^2+R^2\right)/R_f^2, \quad n(r>R)=1. \qquad (4)$$

The potential having this property [35] is

$$V(r\leqslant R)=V_0(r^2/R^2-1), \quad V(r>R)=0, \qquad (5)$$

where $V_0=E(R/R_f)^2$ is the depth at $r=0$. This is a HO potential truncated at $r=R$. The outer region of the nuclear potential has a diffuse surface, and so deviates from the ideal

Luneburg lens. This causes astigmatism to occur, which is nothing but the emergence of a nuclear rainbow. Thus the emergence of the nuclear rainbow is due the properties of both the Luneburg-lens-like potential in the internal region and the diffuse attraction in the outer region. The values of the strength of the potential in Table I are consistent with those evaluated from the constraint of the Pauli principle at $E = 0$, i.e., $V_0 = (N_0 + 3/2)\hbar\omega$, which are 121, 125, 157, and 305 MeV for $\alpha + \alpha$, $\alpha + {}^{16}$O, $\alpha + {}^{40}$Ca, and ^{16}O$+{}^{16}$O, respectively. Thus the deep nature of the potential is a direct consequence of the Pauli principle. This explains why a rainbow occurs in nuclear scattering in the potentials that generate cluster states at lower energies, near the threshold energy. A deep double folding potential derived from a density-dependent effective two-body force, such as the DDM3Y force [26], resembles the Luneburg-lens-like potential and has been successfully used in scattering and structure studies [18,27,30,31,33,34]. According to the present study, for which the depth and shape in the internal region are determined to be constrained by the Pauli principle, it seems that the Pauli principle manifests itself through the density dependence as well as the exchange terms [36–38].

From the structure viewpoint, shell model wave functions in the HO potential, which have almost complete overlaps with the Pauli forbidden states embedded in the local potential as shown in Table I, are equivalent to the cluster representation of Wildermuth and Kanellopoulos [39–41] and can be represented by the SU(3) model [42]. This wave function with a Gaussian tail is damped at the surface. On the other hand, in the present local potential cluster model, which has an attractive potential with an exponential tail at the surface similar to a Woods-Saxon potential, the inner oscillations of the wave function are damped [3–5] due to the orthogonality to the Pauli forbidden states with $N < N_0$ embedded in the Luneburg-lens-like potential. This brings about the enhancement of the amplitude of the wave function at the surface, i.e., emergence and development of cluster structure. Thus the Pauli principle plays the dual role of causing (i) the *shell model* potential with a deep HO shape as the structural Pauli attraction and (ii) the *cluster structure* with the damped inner oscillations and enhanced surface amplitude by the orthogonality to the embedded Pauli forbidden states due to (i).

When two nuclei with a typical shell model structure such as the double magic nucleus α particle, ^{16}O, ^{40}Ca, and ^{208}Pb come closer, the universal Pauli attraction inevitably makes possible the emergence of a cluster structure slightly above the highest Pauli-forbidden state because of the diffuse surface, i.e., near the threshold energy of the compound system. This is the reason why the α cluster structure typically appears for the double magic core $+$ α systems like ^{8}Be, ^{20}Ne, ^{44}Ti, and ^{212}Po. The shell model structure of the internal constituent nuclei (dynamical nature) and the existence of redundant Pauli forbidden states due to the Pauli principle in the wave functions of the relative motion (kinematical nature) are closely interrelated for the emergence of both the cluster structures in the compound system and nuclear rainbows. The Pauli principle does not only provide the *raison d'être* for the shell structure of nuclei but also for the emergence of the cluster structure near the threshold. This will not be limited to closed nuclei and two nuclear systems as long as redundant Pauli forbidden states exist. Also, the nucleon-nucleon potential may have a strong Pauli attraction due to the Pauli principle rather than the repulsive core [7,43,44], the effects of which could be seen in few body systems.

To summarize, the existence of a Luneburg-lens-like universal structural Pauli attraction in the internal region of nucleus-nucleus interaction has been shown. This is different from the traditional view that a structural repulsive core exists at short distances. It is found that the depth and the shape of the potential in the internal region is constrained to a Luneburg-lens-like truncated harmonic oscillator potential by the Pauli principle. The present work reinforces the empirical threshold rule, which had intuitively been understood to be due to the saturation property of the nuclear force. The emergence of a cluster state near the threshold energy can now be seen as a consequence of both the Pauli principle in the internal region and diffuse attraction in the outer region. The emergence of cluster structures and rainbows are unified as a consequence of a Luneburg-lens-like universal structural Pauli attraction in the internal region (kinematical) and diffuse attraction in the outer region (dynamical).

The author thanks the Yukawa Institute for Theoretical Physics, Kyoto University for the hospitality extended during a stay in February 2016 where this work was completed.

[1] A. Bohr and B. R. Mottelson, *Nuclear Structure*, Vol. I (W. A. Benjamin, New York, 1969).
[2] I. Shimodaya, R. Tamagaki, and H. Tanaka, Prog. Theor. Phys. **27**, 793 (1962); **25**, 853 (1961).
[3] R. Tamagaki and H. Tanaka, Prog. Theor. Phys. **34**, 191 (1965).
[4] R. Tamagaki, Prog. Theor. Phys. Suppl. **E68**, 242 (1968), and references therein.
[5] J. Hiura and R. Tamagaki, Suppl. Prog. Theor. Phys. **52**, 25 (1972).
[6] S. Ali and A. R. Bodmer, Nucl. Phys. A **80**, 99 (1966).
[7] S. Otsuki, R. Tamagaki, and M. Yasuno, in *Commemoration Issue for the 30th Anniversary of the Meson Theory by Dr. H. Yukawa*, special issue of Prog. Theor. Phys. Suppl. **E65**, 578 (1965).
[8] A. Tohsaki, F. Tanabe, and R. Tamagaki, Prog. Theor. Phys. **53**, 1022 (1975).
[9] T. Ando, K. Ikeda, and A. Tohsaki-Suzuki, Prog. Theor. Phys. **59**, 306 (1978).
[10] B. Buck, H. Friedrich, and C. Wheatley, Nucl. Phys. A **275**, 246 (1977).
[11] P. E. Hodgson, *Nuclear Reactions and Nuclear Structure* (Clarendon Press, Oxford, 1971); Nuclear Heavy Ion Reactions (Clarendon Press, Oxford, 1978).
[12] D. M. Brink, *Semi-classical Methods for Nucleus-Nucleus Scattering* (Cambridge University Press, Cambridge, 1985).
[13] S. Ohkubo, Y. Kondo, and S. Nagata, Prog. Theor. Phys. **57**, 82 (1977).

[14] F. Michel, J. Albinski, P. Belery, T. Delbar, G. Grégoire, B. Tasiaux, and G. Reidemeister, Phys. Rev. C **28**, 1904 (1983).
[15] F. Michel and P. Vanderpoorten, Phys. Rev. C **16**, 142 (1977).
[16] T. Delbar, G. Grégoire, G. Paic, R. Ceuleneer, F. Michel, R. Vanderpoorten, A. Budzanowski, H. Dabrowski, L. Freindl, K. Grotowski, S. Micek, R. Planeta, A. Strzalkowski, and K. A. Eberhard, Phys. Rev. C **18**, 1237 (1978).
[17] E. Stiliaris *et al.*, Phys. Lett. B **223**, 291 (1989).
[18] D. T. Khoa, W. von Oertzen, H. G. Bohlen, and S. Ohkubo, J. Phys. G **34**, R111 (2007), and references therein.
[19] F. Michel, S. Ohkubo, and G. Reidemeister, Prog. Theor. Phys. Suppl. **132**, 7 (1998); S. Ohkubo, T. Yamaya, and P. E. Hodgson, in *Nucleon-Hadron Many-Body Systems*, edited by H. Ejiri and H. Toki (Oxford University Press, Oxford, 1999), p. 150, and references therein.
[20] F. Michel, G. Reidemeister, and S. Ohkubo, Phys. Rev. Lett. **57**, 1215 (1986); Phys. Rev. C **37**, 292 (1988).
[21] S. Ohkubo, Phys. Rev. C **38**, 2377 (1988).
[22] F. Michel, G. Reidemeister, and S. Ohkubo, Phys. Rev. C **34**, 1248 (1986).
[23] T. Yamaya, S. Oh-ami, M. Fujiwara, T. Itahashi, K. Katori, M. Tosaki, S. Kato, S. Hatori, and S. Ohkubo, Phys. Rev. C **42**, 1935 (1990).
[24] T. Yamaya, K. Katori, M. Fujiwara, S. Kato, and S. Ohkubo, Prog. Theor. Phys. Suppl. **132**, 73 (1998).
[25] A. Hasegawa and S. Nagata, Prog. Theor. Phys. **45**, 1786 (1971); Y. Yamamoto, *ibid.* **52**, 471 (1974).
[26] A. M. Kobos *et al.*, Nucl. Phys. A **384**, 65 (1982); **425**, 205 (1984).
[27] U. Atzrott, P. Mohr, H. Abele, C. Hillenmayer, and G. Staudt, Phys. Rev. C **53**, 1336 (1996).
[28] J. Albiński and F. Michel, Phys. Rev. C **25**, 213 (1982).
[29] F. Michel, G. Reidemeister, and S. Ohkubo, Phys. Rev. C **63**, 034620 (2001); F. Michel, F. Brau, G. Reidemeister, and S. Ohkubo, Phys. Rev. Lett. **85**, 1823 (2000).
[30] H. Abele and G. Staudt, Phys. Rev. C **47**, 742 (1993).
[31] Y. Hirabayashi and S. Ohkubo, Phys. Rev. C **88**, 014314 (2013) and references therein.
[32] S. Ohkubo and K. Yamashita, Phys. Rev. C **66**, 021301(R) (2002).
[33] D. T. Khoa, W. von Oertzen, H. G. Bohlen, and F. Nuoffer, Nucl. Phys. A **672**, 387 (2000).
[34] M. P. Nicoli, F. Haas, R. M. Freeman, N. Aissaoui, C. Beck, A. Elanique, R. Nouicer, A. Morsad, S. Szilner, Z. Basrak, M. E. Brandan, and G. R. Satchler, Phys. Rev. C **60**, 064608 (1999).
[35] F. Michel, G. Reidemeister, and S. Ohkubo, Phys. Rev. Lett. **89**, 152701 (2002).
[36] D. T. Khoa, Nucl. Phys. A **484**, 386 (1988).
[37] S. K. Gupta and B. Sinha, Phys. Rev. C **30**, 1093 (1984).
[38] A. K. Chaudhuri, D. N. Basu, and B. Sinha, Nucl. Phys. A **439**, 415 (1985); A. K. Chaudhuri and B. Sinha, *ibid.* **455**, 169 (1986).
[39] K. Wildermuth and Th. Kanellopoulos, Nucl. Phys. **7**, 150 (1958); **9**, 449 (1958/59).
[40] K. Wildermuth and W. McClure, *Cluster Representation of Nuclei*, Springer Tracts in Modern Physics, Vol. 41 (Springer-Verlag, Berlin, 1966).
[41] B. F. Bayman and A. Bohr, Nucl. Phys. **9**, 596 (1958/59).
[42] J. P. Elliott, Proc. R. Soc. London A **245**, 562 (1958).
[43] S. Otsuki, R. Tamagaki, and M. Wada, Prog. Theor. Phys. **32**, 220 (1964); S. Machida and M. Namiki, *ibid.* **33**, 125 (1965).
[44] S. Aoki, J. Balog, and P. Weisz, Prog. Theor. Phys. **128**, 1269 (2012).